An Upper Limit on the Amplitude of Stochastic Gravitational-Wave Background of Cosmological Origin

The LIGO Scientific Collaboration and the Virgo Collaboration

A stochastic background of gravitational waves is expected to arise from a superposition of a large number of unresolved gravitational-wave sources of astrophysical and cosmological origin. It is expected to carry unique signatures from the earliest epochs in the evolution of the universe, inaccessible to the standard astrophysical observations [1]. Direct measurements of the amplitude of this background therefore are of fundamental importance for understanding the evolution of the universe when it was younger than one minute. Here we report direct limits on the amplitude of the stochastic gravitational-wave background using the data from a two-year science run of the Laser Interferometer Gravitational-wave Observatory (LIGO) [2]. Our result constrains the energy density of the stochastic gravitational-wave background normalized by the critical energy density of the universe, in the frequency band around 100 Hz, to be less than 6.9×10^{-6} at 95% confidence. The data rule out models of early universe evolution with relatively large equation-of-state parameter [3], as well as cosmic (super)string models with relatively small string tension [4] that are favoured in some string theory models [5]. This search for the stochastic background improves upon the indirect limits from the Big Bang Nucleosynthesis [1, 6] and cosmic microwave background [7] at 100 Hz.

According to the general theory of relativity, gravitational waves (GWs) are produced by accelerating mass distributions with a quadrupole (or higher) moment. Moreover, in the early phases of the evolution of the universe, they can be produced by the mechanism of amplification of vacuum fluctuations. Once produced, GWs travel through space-time at the speed of light, and are essentially unaffected by the matter they encounter. As a result, GWs emitted shortly after the Big Bang (and observed today) would carry unaltered information about the physical processes that generated them. These waves are expected to be generated by a large number of unresolved sources, forming a stochastic gravitational-wave background (SGWB) that is usually described in terms of the GW spectrum:

$$\Omega_{\mathrm{GW}}(f) = \frac{f}{\rho_c} \frac{d\rho_{\mathrm{GW}}}{df} , \tag{1}$$

where $d\rho_{\mathrm{GW}}$ is the energy density of gravitational radiation contained in the frequency range f to $f + df$ and ρ_c is the critical energy density of the universe [8]. Many cosmological mechanisms for generation of the SGWB exist, such as the inflationary models [9, 10], pre-big-bang models [11–13], electroweak phase transition [14], and cosmic strings [4, 5, 15, 16]. There are also astrophysical mechanisms, such as due to magnetars [17] or rotating neutron stars [18].

The physical manifestation of GWs consists of stretching and compressing the spatial dimensions orthogonal to the direction of wave propagation, producing strain in an oscillating quadrupolar pattern. A Michelson interferometer with suspended mirrors [2] is well suited to measure this differential strain signal due to GWs. Over the past decade, LIGO has built three such multi-kilometer interferometers, at two locations [2]: H1 (4 km) and H2 (2 km) share the same facility at Hanford, WA, and L1 (4 km) is located in Livingston Parish, LA. LIGO, together with the 3 km interferometer Virgo [19] in Italy and GEO [20] in Germany, forms a network of GW observatories. LIGO has completed the science run S5 (between November 5, 2005 and September 30, 2007), acquiring one year of data coincident among H1, H2 and L1, at the interferometer design sensitivities (Fig. 1).

The search for the SGWB using LIGO data is performed by cross-correlating strain data from pairs of interferometers [8]. In the frequency domain, the cross-correlation between two interferometers is multiplied by a filter function $\tilde{Q}(f)$ (c.f. online supplement):

$$\tilde{Q}(f) = \mathcal{N} \frac{\gamma(f)\Omega_{\mathrm{GW}}(f)H_0^2}{f^3 P_1(f)P_2(f)} . \tag{2}$$

This filter optimizes the signal-to-noise ratio, enhancing the frequencies at which the signal of the template spectrum $\Omega_{\mathrm{GW}}(f)$ is strong, while suppressing the frequencies at which the detector noise ($P_1(f)$ and $P_2(f)$) is large. In Eq. 2, and throughout this letter, we assume the present value of the Hubble parameter $H_0 = 72$ km/s/Mpc [21], and use $\gamma(f)$ to denote the overlap reduction function [8], arising from the overlap of antenna patterns of interferometers at different locations and with different orientations. For the H1-L1 and H2-L1 pairs the sensitivity above roughly 50 Hz is attenuated due to the overlap reduction. Since most theoretical models in the LIGO frequency band are characterized by a power law spectrum, we assume a power law template GW spectrum with index α: $\Omega_{\mathrm{GW}}(f) = \Omega_\alpha (f/100 \text{ Hz})^\alpha$.
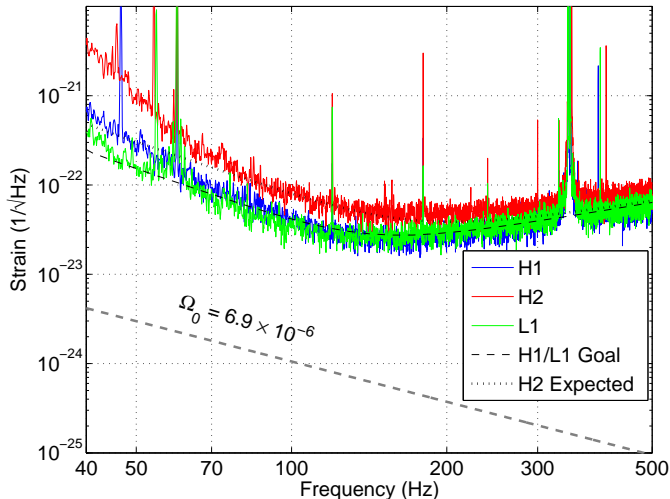
FIG. 1: **Sensitivities of LIGO interferometers.** LIGO interferometers reached their design sensitivity in November 2005, resulting in the interferometer strain noise at the level of 3×10^{-22} rms in a 100 Hz band around 100 Hz. This figure shows typical strain sensitivities of LIGO interferometers during the subsequent science run S5. Also shown is the strain amplitude corresponding to the upper limit on the GW energy density presented in this paper (gray dashed line). Note that this upper limit is ~ 100 times lower than the individual interferometer sensitivities, which illustrates the advantage of using the cross-correlation technique in this analysis.

The normalization constant $\mathcal{N}$ in Eq. 2 is chosen such that the expected value of the optimally filtered cross-correlation is Ω_α.

We apply the above search technique to the data acquired by LIGO during the science run S5. We include two interferometer pairs: H1-L1 and H2-L1. Summing up the contributions to the cross-correlation in the frequency band 41.5-169.25 Hz, which contains 99% of the sensitivity, leads to the final point estimate for the frequency independent GW spectrum ($\alpha = 0$): $\Omega_0 = (2.1 \pm 2.7) \times 10^{-6}$, where the quoted error is statistical. We calculate the Bayesian 95% confidence upper limit for Ω_0, using the previous LIGO result (S4 run [22]) as a prior for Ω_0 and averaging over the interferometer calibration uncertainty. This procedure yields the 95% confidence upper limit $\Omega_0 < 6.9 \times 10^{-6}$. For other values of the power index α in the range between -3 and 3, the 95% upper limit varies between 1.9×10^{-6} and 7.1×10^{-6}. These results constitute more than an order of magnitude improvement over the previous LIGO result in this frequency region [22]. Fig. 2 shows this result in comparison with other observational constraints and some of the cosmological SGWB models.

Prior to the result described here, the most constraining bounds on the SGWB in the frequency band around 100 Hz came from the Big-Bang-Nucleosynthesis (BBN) and from cosmic microwave background (CMB) measurements. The BBN bound is derived from the fact that a large GW energy density at the time of BBN would alter the abundances of the light nuclei produced in the process. Hence, the BBN model and observations constrain the total GW energy density at the time of nucleosynthesis [1, 6]:

$$\int \Omega_{\mathrm{GW}}(f) \, d(\ln f) < 1.1 \times 10^{-5} \, (N_\nu - 3), \tag{3}$$

where N_ν (the *effective* number of neutrino species at the time of BBN) captures the uncertainty in the radiation content during BBN. Measurements of the light-element abundances, combined with the Wilkinson Microwave Anistropy Probe (WMAP) data give the upper bound $N_\nu - 3 < 1.4$ [23]. Similarly, a large GW background at the time of decoupling of CMB would alter the observed CMB and matter power spectra. Assuming homogeneous initial conditions, the total GW energy density at the time of CMB decoupling is constrained to $\int \Omega_{\mathrm{GW}}(f) \, d(\ln f) < 1.3 \times 10^{-5}$ [7]. In the LIGO frequency band and for $\alpha = 0$, these bounds become: $\Omega_0^{\mathrm{BBN}} < 1.1 \times 10^{-5}$ and $\Omega_0^{\mathrm{CMB}} < 9.5 \times 10^{-6}$. Our result has now surpassed these bounds, which is one of the major milestones that LIGO was designed to achieve. Moreover, the BBN and CMB bounds apply only to backgrounds generated prior to the BBN and the CMB decoupling respectively, while the LIGO bound also probes the SGWB produced later (this is the case, for example, in cosmic strings models).

Our result also constrains models of the early universe evolution. While the evolution of the universe following the BBN is well understood, there is little observational data probing the evolution prior to BBN, when the universe was
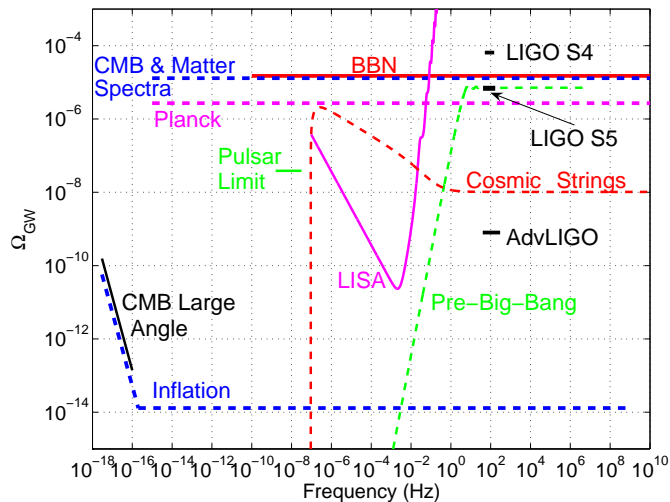
FIG. 2: **Comparison of different SGWB measurements and models.** The result presented here (LIGO S5) applies in the frequency band around 100 Hz, and is compared to the previous LIGO S4 result [22] and to the projected Advanced LIGO sensitivity [24] in this band. The indirect bounds due to BBN [1, 6] and CMB and matter power spectra [7] apply to the integral of $\Omega_{\rm GW}(f)$ over the frequency bands denoted by the corresponding dashed curves. Projected sensitivities of the satellite-based Planck CMB experiment [7] and LISA GW detector [25] are also shown. The pulsar bound [26] is based on the fluctuations in the pulse arrival times of millisecond pulsars and applies at frequencies around 10^{-8} Hz. Measurements of the CMB at large angular scales constrain the possible redshift of CMB photons due to the SGWB, and therefore limit the amplitude of the SGWB at largest wavelengths (smallest frequencies) [6]. Examples of inflationary [9, 10], cosmic strings [4, 5, 15, 16], and pre-big-bang [11–13] models are also shown (the amplitude and the spectral shape in these models can vary significantly as a function of model parameters).

less than one minute old. The GW spectrum $\Omega_{\rm GW}(f)$ carries information about exactly this epoch in the evolution. In particular, measuring $\Omega_{\rm GW}(f)$ is the best way to test for existence of presently unknown "stiff" energy components in the early universe [3], for which a small density variation is associated with a large pressure change, which could carry information about the physics of the inflationary era [27]. Fig. 3 demonstrates how the result presented here can be used to constrain the existence of these new energy components.

Our result also constrains models of cosmic (super)strings. Cosmic strings were originally proposed as topological defects formed during phase transitions in the early universe [15]. More recently, it was realized that fundamental strings may also be expanded to cosmological scales [5]. Hence, searching for cosmic strings may provide a unique and powerful window into string theory and into particle physics at the highest energy scales. Fig. 4 shows that our result, along with other observations, can be used to constrain the parameters in the cosmic string models. While our result is currently excluding a fraction of the allowed parameter space, Advanced LIGO [24] is expected to probe most of these models.

Measurements of the SGWB also offer the possibility of probing alternative models of the early universe cosmology. For example, in the pre-Big-Bang model [11–13] the universe starts off large and then undergoes a period of inflation driven by the kinetic energy of a dilaton field, after which the standard cosmology follows. Although more speculative than the standard cosmology model, the pre-Big-Bang model makes testable predictions of the GW spectrum. As shown in Fig. 5, the BBN and CMB bounds are currently the most constraining for this model and Advanced LIGO [24] is expected to surpass them.

[1] Maggiore, M., Gravitational wave experiments and early universe cosmology, *Phys. Rep.* **331**, 283-367 (2000).
[2] Abbott B. et al., Detector description and performance for the first coincidence observations between LIGO and GEO, *Nucl. Instr. Meth. A* **517**, 154-179 (2004).
[3] Boyle L. and Buonanno A., Relating gravitational wave constraints from primordial nucleosynthesis, pulsar timing, laser interferometers, and the CMB: Implications for the early universe, *Phys. Rev. D* **78**, 043531 (2008).
[4] Siemens X., Mandic V., and Creighton J., Gravitational-Wave Stochastic Background from Cosmic Strings, *Phys. Rev. Lett.* **98**, 111101 (2007).
[5] S. Sarangi and S. H. H. Tye, Cosmic string production towards the end of brane inflation, *Phys. Lett. B* **536**, 185-192

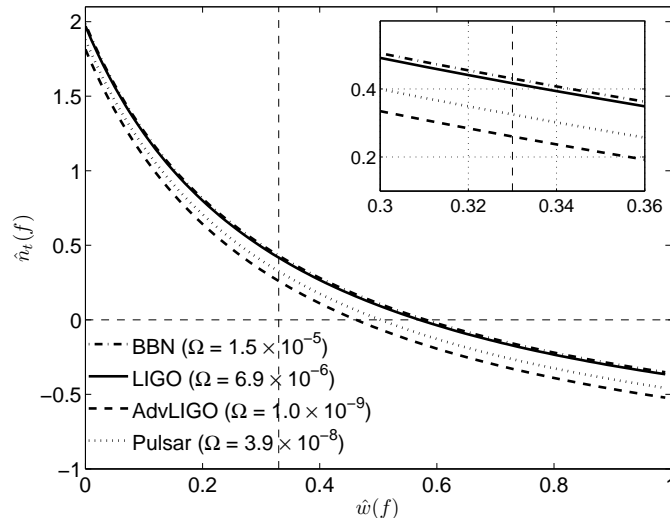FIG. 3: **Constraining early universe evolution.** The GW spectrum $\Omega_{GW}(f)$ is related to the parameters that govern the evolution of the universe [3]:
$\Omega_{GW}(f) = A\, f^{\hat{\alpha}(f)}\, f^{\hat{n}_t(f)}\, r$, where $\hat{\alpha}(f) = 2\,\frac{3\hat{w}(f)-1}{3\hat{w}(f)+1}$, r is the ratio of tensor and scalar perturbation amplitudes (measured by the cosmic microwave background (CMB) experiments), $\hat{n}_t(f)$ and $\hat{w}(f)$ are effective (average) tensor tilt and equation of state parameters respectively, and A is a constant depending on various cosmological parameters. Hence, the measurements of Ω_{GW} and r can be used to place constraints in the $\hat{w} - \hat{n}_t$ plane, *independently* of the cosmological model. The figure shows the $\hat{w} - \hat{n}_t$ plane for $r = 0.1$. The regions excluded by the BBN [23], LIGO, and pulsar [26] bounds are above the corresponding curves (the inset shows a zoom-in on the central part of the figure). The BBN curve was calculated in [3]. We note that the CMB bound [7] almost exactly overlaps with the BBN bound. Also shown is the expected reach of Advanced LIGO [24]. Note that these bounds apply to different frequency bands, so their direct comparison is meaningful only if $\hat{n}_t(f)$ and $\hat{w}(f)$ are frequency independent. We note that for the simplest single-field inflationary model that still agrees with the cosmological data, $V(\phi) = m^2\phi^2/2$, $r = 0.14$ and $n_t(100\,\mathrm{Hz}) = -0.035$ [28], implying a LIGO bound on the equation-of-state parameter of $\hat{w}(100\,\mathrm{Hz}) < 0.59$.

(2002).

[6] Allen, B., The stochastic gravity-wave background: sources and detection, preprint arXiv:gr-qc/9604033 (1996).

[7] Smith, T.L., Pierpaoli, E., and Kamionkowski, M., A new cosmic microwave background constraint to primordial gravitational waves, *Phys. Rev. Lett.* **97**, 021301 (2006).

[8] Allen, B. and Romano, J., Detecting a stochastic background of gravitational radiation: Signal processing strategies and sensitivities, *Phys. Rev. D* **59**, 102001 (1999).

[9] Starobinskii, A.A., Spectrum of relict gravitational radiation and the early state of the universe, *JETP Lett.* **30**, 682 (1979).

[10] Bar-Kana, R., Limits on direct detection of gravitational waves, *Phys. Rev. D* **50**, 1157 (1994).

[11] Brustein, R. et al, Relic gravitational waves from string cosmology, *Phys. Lett. B* **361**, 45-51 (1995).

[12] Buonanno, A. et al, Spectrum of relic gravitational waves in string cosmology, *Phys. Rev. D* **55**, 3330-3336 (1997).

[13] Mandic, V. & Buonanno, A., Accessibility of the pre-big-bang models to LIGO, *Phys. Rev. D* **73**, 063008 (2006).

[14] Apreda, R. et al, Gravitational waves from electroweak phase transitions, *Nucl. Phys. B* **631**, 342-368 (2002).

[15] Kibble, T.W.B., Topology of cosmic domains and strings, *J. Phys. A* **9**, 1387-1398 (1976).

[16] Damour, T. & Vilenkin A., Gravitational radiation from cosmic (super)strings: Bursts, stochastic background, and observational windows, *Phys. Rev. D* **71**, 063510 (2005).

[17] Regimbau, T. & de Freitas Pacheco, J.A., Gravitational wave background from magnetars, *Astron. and Astrophys.* **447**, 1-8 (2006).

[18] Regimbau, T. & de Freitas Pacheco, J.A., Cosmic background of gravitational waves from rotating neutron stars, *Astron. and Astrophys.* **376**, 381-385 (2001).

[19] Acernese, F. et al., Status of Virgo, *Class. Quant. Grav.* **25**, 114045 (2008).

[20] Willke, B. et al., The GEO-HF project, *Class. Quant. Grav.* **23**, S207-S214 (2006).

[21] Bennet, C.L. et al., First-Year *Wilkinson Microwave Anisotropy Probe (WMAP)* Observations: Preliminary Maps and Basic Results, *Astrophys. J. Suppl.* **148**, 1-28 (2003).

[22] Abbott B. et al., Searching for a Stochastic Background of Gravitational Waves with the Laser Interferometer Gravitational-Wave Observatory, *Astrophys. J.* **659**, 918-930 (2007).

[23] Cyburt, R.H. et al, New BBN limits on physics beyond the standard model from ^{4}He, *Astropart. Phys.* **23**, 313-323 (2005).

[24] Advanced LIGO Team, Advanced LIGO Reference Design, LIGO preprint, (2007)
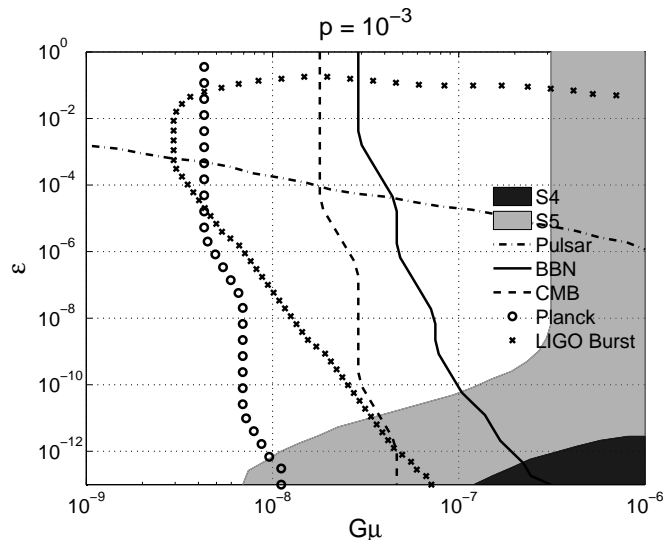http://www.ligo.caltech.edu/docs/M/M060056-10.pdf.

FIG. 4: **Cosmic strings models.** The network of cosmic strings is usually parametrized by the string tension μ (multiplied by the Newton constant G), and reconnection probability p. The CMB observations limit $G\mu < 10^{-6}$. If the size of the cosmic string loops is determined by the gravitational back-reaction [29], the size of the loop can be parametrized by a parameter ϵ [16] which is essentially unconstrained. The mechanism for production of GWs relies on cosmic string cusps: regions of string that move at speeds close to the speed of light. If the cusp motion points toward Earth, a detectable burst of gravitational radiation may be produced [16, 30]. The superposition of GWs from all string cusps in the cosmic string network would produce a SGWB [4]. This figure shows how different experiments probe the $\epsilon - G\mu$ plane for a typical value of $p = 10^{-3}$ [4] (p is expected to be in the range $10^{-4} - 1$). The excluded regions (always to the right of the corresponding curves) correspond to the S4 LIGO result [22], this result, BBN bound [6, 23], CMB bound [7], and the pulsar limit [26]. In particular, the bound presented in this paper excludes a new region in this plane ($7 \times 10^{-9} < G\mu < 1.5 \times 10^{-7}$ and $\epsilon < 8 \times 10^{-11}$), which is not accessible to any of the other measurements. Also shown is the expected sensitivity for the search for individual bursts from cosmic string cusps with LIGO S5 data [30]. The region to the right of this curve is expected to produce at least one cosmic string burst event detectable by LIGO during the S5 run. Note that this search is complementary to the search for the SGWB as it probes a different part of the parameter space. Also shown is the region that will be probed by the Planck satellite measurements of the CMB [7]. The entire plane shown here will be accessible to Advanced LIGO [24] SGWB search.

[25] Bender, P.L., Danzmann, K., and the LISA Study Team, Laser Interferometer Space Antenna for the detection and observation of gravitational waves: Pre-phase A report, 2nd Edition, Max-Plank Institut fuer Quantenoptik, MPQ233 (1998).

[26] Jenet, F.A. et al., Upper Bounds on the Low-Frequency Stochastic Gravitational Wave Background from Pulsar Timing Observations: Current Limits and Future Prospects, *Astrophys. J.* **653**, 1571-1576 (2006).

[27] Grishchuk, L.P. and Sidorov, Yu.V., Squeezed quantum states of relic gravitons and primordial density fluctuations, *Phys. Rev. D* **42**, 3413-3421 (1990).

[28] Komatsu, E. et al., Five-Year Wilkinson Microwave Anisotropy Probe (WMAP) Observations: Cosmological Interpretation, *Astrophys. J. Suppl.* **180**, 330-376 (2009).

[29] Siemens, X. et al, Size of the smallest scales in cosmic string networks, *Phys. Rev. D* **66**, 043501 (2002).

[30] Siemens, X. et al., Gravitational wave bursts from cosmic (super)strings: Quantitative analysis and constraints, *Phys. Rev D* **73**, 105001 (2006).

Supplementary Information is linked to the online version of the paper at www.nature.com/nature.
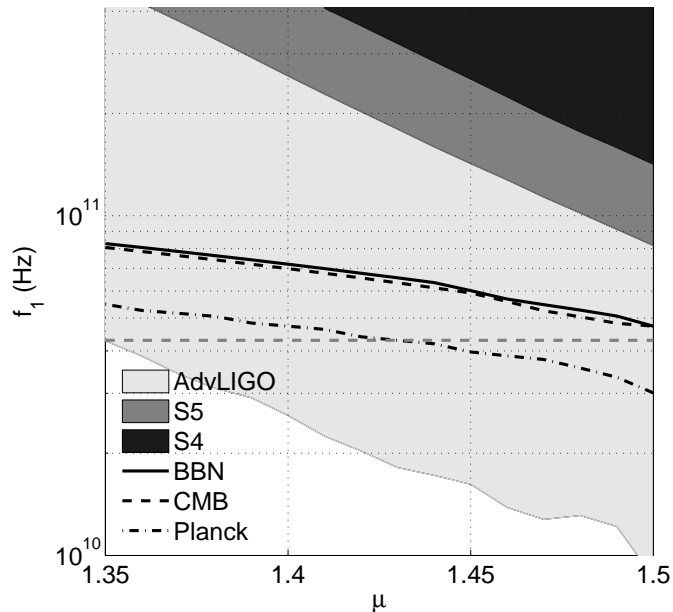
FIG. 5: **Pre-Big-Bang models.** In the pre-Big-Bang model, the GWs are produced via the mechanism of amplification of vacuum fluctuations, analogously to the standard inflationary model. The typical GW spectrum increases as f^3 up to a turn-over frequency f_s, above which $\Omega_{\mathrm{GW}}(f) \sim f^{3-2\mu}$ with $\mu < 1.5$. The spectrum cuts off at a frequency f_1, which is theoretically expected to be within a factor of 10 from 4.3×10^{10} Hz (dashed horizontal line). This figure shows the $f_1 - \mu$ plane for a representative value of $f_s = 30$ Hz. Excluded regions corresponding to the S4 result and to the result presented here are shaded. The regions excluded by the BBN [6, 23] and the CMB [7] bounds are above the corresponding curves. The expected reaches of the Advanced LIGO [24] and of the Planck satellite [7] are also shown.

document number LIGO-P080099-12-Z.

Author Contributions are listed in Supplementary Information.

Author Information: Reprints and permissions information is available at npg.nature.com/reprintsandpermissions. Correspondence and requests for materials should be addressed to V. Mandic (mandic@physics.umn.edu).

B. P. Abbott[1], R. Abbott[1], F. Acernese[2ac], R. Adhikari[1],
P. Ajith[3], B. Allen[3,4], G. Allen[5], M. Alshourbagy[6ab],
R. S. Amin[7], S. B. Anderson[1], W. G. Anderson[4], F.
Antonucci[8a], S. Aoudia[9], M. A. Arain[10], M. Araya[1],
H. Armandula[1], P. Armor[4], K.G. Arun[11], Y. Aso[1], S. Aston[12],
P. Astone[8a], P. Aufmuth[13], C. Aulbert[3], S. Babak[14], P. Baker[15],
G. Ballardin[16], S. Ballmer[1], C. Barker[17], D. Barker[17], F.
Barone[2ac], B. Barr[18], P. Barriga[19], L. Barsotti[20], M. Barsuglia[21],
M. A. Barton[1], I. Bartos[22], R. Bassiri[18], M. Bastarrika[18], Th.S.
Bauer[23a], B. Behnke[14], M. Benacquista[24], J. Betzwieser[1],
P. T. Beyersdorf[25], S. Bigotta[6ab], I. A. Bilenko[26], G. Billingsley[1],
S. Birindelli[9], R. Biswas[4], M.A. Bizouard[11], E. Black[1],
J. K. Blackburn[1], L. Blackburn[20], D. Blair[19], B. Bland[17], C.
Boccara[27], T. P. Bodiya[20], L. Bogue[28], F. Bondu[9], L. Bonelli[6ab],
R. Bork[1], V. Boschi[1], S. Bose[29], L. Bosi[30a], S. Braccini[6a], C.
Bradaschia[6a], P. R. Brady[4], V. B. Braginsky[26], J.F.J. van den
Brand[23ab], J. E. Brau[31], D. O. Bridges[28], A. Brillet[9],
M. Brinkmann[3], V. Brisson[11], C. Van Den Broeck[32],
A. F. Brooks[1], D. A. Brown[33], A. Brummit[34], G. Brunet[20],
A. Bullington[5], H.J. Bulten[23ab], A. Buonanno[35],
O. Burmeister[3], D. Buskulic[36], R. L. Byer[5], L. Cadonati[37], G.
Cagnoli[38a], E. Calloni[2ab], J. B. Camp[39], E. Campagna[38ac],
J. Cannizzo[39], K. C. Cannon[1], B. Canuel[16], J. Cao[20], F.
Carbognani[16], L. Carbone[30a], L. Cardenas[1], S. Caride[40],
G. Castaldi[41], S. Caudill[7], M. Cavaglià[42], F. Cavalier[11], R.
Cavalieri[16], G. Cella[6a], C. Cepeda[1], T. Chalermsongsak[1],
E. Chalkley[18], P. Charlton[43], E. Chassande-Mottin[21],
S. Chatterji[1,8a], S. Chelkowski[12], Y. Chen[14,44], N. Christensen[45],
C. T. Y. Chung[46], D. Clark[5], J. Clark[32], J. H. Clayton[4], F.
Cleva[9], E. Coccia[47ab], T. Cokelaer[32], C. N. Colacino[48], J.
Colas[16], M. Colombini[8b], R. Conte[49], D. Cook[17],
T. R. C. Corbitt[20], C. Corda[6ab], N. Cornish[15], A. Corsi[8a], J.-P.
Coulon[9], D. Coward[19], D. C. Coyne[1], J. D. E. Creighton[4],
T. D. Creighton[24], A. M. Cruise[12], R. M. Culter[12],
A. Cumming[18], L. Cunningham[18], E. Cuoco[16],
S. L. Danilishin[26], S. D'Antonio[47a], K. Danzmann[3,13], A.
Dari[30ab], V. Dattilo[16], B. Daudert[1], M. Davier[11], G. Davies[32],
E. J. Daw[50], R. De Rosa[2ab], D. DeBra[5], J. Degallaix[3], M. del
Prete[6ac], V. Dergachev[40], S. Desai[51], R. DeSalvo[1],
S. Dhurandhar[52], L. Di Fiore[2a], A. Di Lieto[6ab], M. Di Paolo

Emilio[47ad], A. Di Virgilio[6a], M. Díaz[24], A. Dietz[32], F. Donovan[20],
K. L. Dooley[10], E. E. Doomes[53], R. W. P. Drever[54], J. Dueck[3],
I. Duke[20], J. -C. Dumas[19], J. G. Dwyer[22], C. Echols[1],
M. Edgar[18], A. Effler[17], P. Ehrens[1], G. Ely[45], E. Espinoza[1],
T. Etzel[1], M. Evans[20], T. Evans[28], V. Fafone[47ab], S. Fairhurst[32],
Y. Faltas[10], Y. Fan[19], D. Fazi[1], H. Fehrmann[3], I. Ferrante[6ab], F.
Fidecaro[6ab], L. S. Finn[51], I. Fiori[16], R. Flaminio[55], K. Flasch[4],
S. Foley[20], C. Forrest[56], N. Fotopoulos[4], J.-D. Fournier[9],
A. Franzen[13], S. Frasca[8ab], F. Frasconi[6a], M. Frede[3], M. Frei[57],
Z. Frei[48], A. Freise[12], R. Frey[31], T. Fricke[28], P. Fritschel[20],
V. V. Frolov[28], M. Fyffe[28], V. Galdi[41], L. Gammaitoni[30ab],
J. A. Garofoli[33], F. Garufi[2ab], E. Genin[16], A. Gennai[6a],
I. Gholami[14], J. A. Giaime[7,28], S. Giampanis[3], K. D. Giardina[28],
A. Giazotto[6a], K. Goda[20], E. Goetz[40], L. M. Goggin[4],
G. González[7], M. L. Gorodetsky[26], S. Goßler[3], R. Gouaty[7], M.
Granata[21], V. Granata[36], A. Grant[18], S. Gras[19], C. Gray[17],
M. Gray[58], R. J. S. Greenhalgh[34], A. M. Gretarsson[59], C.
Greverie[9], F. Grimaldi[20], R. Grosso[24], H. Grote[3],
S. Grunewald[14], M. Guenther[17], G. Guidi[38ac], E. K. Gustafson[1],
R. Gustafson[40], B. Hage[13], J. M. Hallam[12], D. Hammer[4],
G. D. Hammond[18], C. Hanna[1], J. Hanson[28], J. Harms[60],
G. M. Harry[20], I. W. Harry[32], E. D. Harstad[31], K. Haughian[18],
K. Hayama[24], J. Heefner[1], H. Heitmann[9], P. Hello[11],
I. S. Heng[18], A. Heptonstall[1], M. Hewitson[3], S. Hild[12],
E. Hirose[33], D. Hoak[28], K. A. Hodge[1], K. Holt[28],
D. J. Hosken[61], J. Hough[18], D. Hoyland[19], D. Huet[16],
B. Hughey[20], S. H. Huttner[18], D. R. Ingram[17], T. Isogai[45],
M. Ito[31], A. Ivanov[1], B. Johnson[17], W. W. Johnson[7],
D. I. Jones[62], G. Jones[32], R. Jones[18], L. Sancho de la Jordana[63],
L. Ju[19], P. Kalmus[1], V. Kalogera[64], S. Kandhasamy[60],
J. Kanner[35], D. Kasprzyk[12], E. Katsavounidis[20], K. Kawabe[17],
S. Kawamura[65], F. Kawazoe[3], W. Kells[1], D. G. Keppel[1],
A. Khalaidovski[3], F. Y. Khalili[26], R. Khan[22], E. Khazanov[66],
P. King[1], J. S. Kissel[7], S. Klimenko[10], K. Kokeyama[65],
V. Kondrashov[1], R. Kopparapu[51], S. Koranda[4], D. Kozak[1],
B. Krishnan[14], R. Kumar[18], P. Kwee[13], P. La Penna[16],
P. K. Lam[58], M. Landry[17], B. Lantz[5], M. Laval[9], A. Lazzarini[1],
H. Lei[24], M. Lei[1], N. Leindecker[5], I. Leonor[31], N. Leroy[11], N.
Letendre[36], C. Li[44], H. Lin[10], P. E. Lindquist[1],
T. B. Littenberg[15], N. A. Lockerbie[67], D. Lodhia[12], M. Longo[41],
M. Lorenzini[38a], V. Loriette[27], M. Lormand[28], G. Losurdo[38a],
P. Lu[5], M. Lubinski[17], A. Lucianetti[10], H. Lück[3,13],

B. Machenschalk[14], M. MacInnis[20], J.-M. Mackowski[55],
M. Mageswaran[1], K. Mailand[1], E. Majorana[8a], N. Man[9],
I. Mandel[64], V. Mandic[60], M. Mantovani[16], F. Marchesoni[30a], F.
Marion[36], S. Márka[22], Z. Márka[22], A. Markosyan[5],
J. Markowitz[20], E. Maros[1], J. Marque[16], F. Martelli[38ac],
I. W. Martin[18], R. M. Martin[10], J. N. Marx[1], K. Mason[20], A.
Masserot[36], F. Matichard[7], L. Matone[22], R. A. Matzner[57],
N. Mavalvala[20], R. McCarthy[17], D. E. McClelland[58],
S. C. McGuire[53], M. McHugh[68], G. McIntyre[1],
D. J. A. McKechan[32], K. McKenzie[58], M. Mehmet[3],
A. Melatos[46], A. C. Melissinos[56], G. Mendell[17],
D. F. Menéndez[51], F. Menzinger[16], R. A. Mercer[4],
S. Meshkov[1], C. Messenger[3], M. S. Meyer[28], C. Michel[55], L.
Milano[2ab], J. Miller[18], J. Minelli[51], Y. Minenkov[47a], Y. Mino[44],
V. P. Mitrofanov[26], G. Mitselmakher[10], R. Mittleman[20],
O. Miyakawa[1], B. Moe[4], M. Mohan[16], S. D. Mohanty[24],
S. R. P. Mohapatra[37], J. Moreau[27], G. Moreno[17], N. Morgado[55],
L. Carbone[47ab], T. Morioka[65], K. Mors[3], S. Mosca[2ab],
K. Mossavi[3], B. Mours[36], C. MowLowry[58], G. Mueller[10],
D. Muhammad[28], H. zur Mühlen[13], S. Mukherjee[24],
H. Mukhopadhyay[52], A. Mullavey[58], H. Müller-Ebhardt[3],
J. Munch[61], P. G. Murray[18], E. Myers[17], J. Myers[17], T. Nash[1],
J. Nelson[18], I. Neri[30ab], G. Newton[18], A. Nishizawa[65], F.
Nocera[16], K. Numata[39], E. Ochsner[35], J. O'Dell[34], G. H. Ogin[1],
B. O'Reilly[28], R. O'Shaughnessy[51], D. J. Ottaway[61],
R. S. Ottens[10], H. Overmier[28], B. J. Owen[51], G. Pagliaroli[47ab],
C. Palomba[8a], Y. Pan[35], C. Pankow[10], F. Paoletti[6a,16],
M. A. Papa[4,14], V. Parameshwaraiah[17], S. Pardi[2ab], A.
Pasqualetti[16], R. Passaquieti[6ab], D. Passuello[6a], P. Patel[1],
M. Pedraza[1], S. Penn[69], A. Perreca[12], G. Persichetti[2ab], F.
Piergiovanni[38ac], V. Pierro[41], L. Pinard[55], I. M. Pinto[41],
M. Pitkin[18], H. J. Pletsch[3], M. V. Plissi[18], R. Poggiani[6ab],
F. Postiglione[49], M. Principe[41], R. Prix[3], L. Prokhorov[26],
O. Punken[3], M. Punturo[30a], P. Puppo[8a], S. van der Putten[23a],
V. Quetschke[10], F. J. Raab[17], O. Rabaste[21], D. S. Rabeling[58],
H. Radkins[17], P. Raffai[48], Z. Raics[22], N. Rainer[3],
M. Rakhmanov[24], P. Rapagnani[8ab], V. Raymond[64],
C. M. Reed[17], T. Reed[70], T. Regimbau[9], H. Rehbein[3],
S. Reid[18], D. H. Reitze[10], F. Ricci[8ab], R. Riesen[28], K. Riles[40],
B. Rivera[17], P. Roberts[71], N. A. Robertson[1,18], C. Robinson[32],
E. L. Robinson[14], A. Rocchi[47a], S. Roddy[28], L. Rolland[36],
J. Rollins[22], J. D. Romano[24], R. Romano[2ac], J. H. Romie[28],

C. Röver[3], S. Rowan[18], A. Rüdiger[3], P. Ruggi[16], P. Russell[1],
K. Ryan[17], S. Sakata[65], V. Sandberg[17], V. Sannibale[1],
L. Santamaría[14], S. Saraf[72], P. Sarin[20], B. Sassolas[55],
B. S. Sathyaprakash[32], S. Sato[65], M. Satterthwaite[58],
P. R. Saulson[33], R. Savage[17], P. Savov[44], M. Scanlan[70],
R. Schilling[3], R. Schnabel[3], R. Schofield[31], B. Schulz[3],
B. F. Schutz[14,32], P. Schwinberg[17], J. Scott[18], S. M. Scott[58],
A. C. Searle[1], B. Sears[1], F. Seifert[3], D. Sellers[28],
A. S. Sengupta[1], D. Sentenac[16], A. Sergeev[66], B. Shapiro[20],
P. Shawhan[35], D. H. Shoemaker[20], A. Sibley[28], X. Siemens[4],
D. Sigg[17], S. Sinha[5], A. M. Sintes[63], B. J. J. Slagmolen[58],
J. Slutsky[7], M. V. van der Sluys[64], J. R. Smith[33], M. R. Smith[1],
N. D. Smith[20], K. Somiya[44], B. Sorazu[18], A. Stein[20],
L. C. Stein[20], S. Steplewski[29], A. Stochino[1], R. Stone[24],
K. A. Strain[18], S. Strigin[26], A. Stroeer[39], A. L. Stuver[28],
T. Z. Summerscales[71], K. -X. Sun[5], M. Sung[7], P. J. Sutton[32],
B.L. Swinkels[16], G. P. Szokoly[48], D. Talukder[29], L. Tang[24],
D. B. Tanner[10], S. P. Tarabrin[26], J. R. Taylor[3], R. Taylor[1], R.
Terenzi[47ac], J. Thacker[28], K. A. Thorne[28], K. S. Thorne[44],
A. Thüring[13], K. V. Tokmakov[18], A. Toncelli[6ab], M. Tonelli[6ab],
C. Torres[28], C. Torrie[1], E. Tournefier[36], F. Travasso[30ab],
G. Traylor[28], M. Trias[63], J.Trummer[36], D. Ugolini[73], J. Ulmen[5],
K. Urbanek[5], H. Vahlbruch[13], G. Vajente[6ab], M. Vallisneri[44],
S. Vass[1], R. Vaulin[4], A. Vecchio[12], A. A. van Veggel[18],
J. Veitch[12], P. Veitch[61], C. Veltkamp[3], D. Verkindt[36], F.
Vetrano[38ac], A. Viceré[38ac], A. Villar[1], J.-Y. Vinet[9], H. Vocca[30a],
C. Vorvick[17], S. P. Vyachanin[26], S. J. Waldman[20], L. Wallace[1],
R. L. Ward[1], M.Was[11], A. Weidner[3], M. Weinert[3],
A. J. Weinstein[1], R. Weiss[20], L. Wen[19,44], S. Wen[7], K. Wette[58],
J. T. Whelan[14,74], S. E. Whitcomb[1], B. F. Whiting[10],
C. Wilkinson[17], P. A. Willems[1], H. R. Williams[51], L. Williams[10],
B. Willke[3,13], I. Wilmut[34], L. Winkelmann[3], W. Winkler[3],
C. C. Wipf[20], A. G. Wiseman[4], G. Woan[18], R. Wooley[28],
J. Worden[17], W. Wu[10], I. Yakushin[28], H. Yamamoto[1], Z. Yan[19],
S. Yoshida[75], M. Yvert[36], M. Zanolin[59], J. Zhang[40], L. Zhang[1],
C. Zhao[19], N. Zotov[70], M. E. Zucker[20], J. Zweizig[1]

[1,*]LIGO - California Institute of Technology, Pasadena, CA 91125, USA
[2,†]INFN, sezione di Napoli [a]; Università di Napoli 'Federico II'[b] Complesso
Universitario di Monte S.Angelo, I-80126 Napoli; Università di Salerno, Fisciano,
I-84084 Salerno[c], Italy
[3,*]Albert-Einstein-Institut, Max-Planck-Institut für Gravitationsphysik, D-30167
Hannover, Germany
[4,*]University of Wisconsin-Milwaukee, Milwaukee, WI 53201, USA

[5],[*]Stanford University, Stanford, CA 94305, USA

[6],[†]INFN, Sezione di Pisa^a; Università di Pisa^b; I-56127 Pisa; Università di Siena, I-53100 Siena^c, Italy

[7],[*]Louisiana State University, Baton Rouge, LA 70803, USA

[8],[†]INFN, Sezione di Roma^a; Università 'La Sapienza'^{b}, I-00185 Roma, Italy

[9],[†]Departement Artemis, Observatoire de la Côte d'Azur, CNRS, F-06304 Nice, France.

[10],[*]University of Florida, Gainesville, FL 32611, USA

[11],[†]LAL, Université Paris-Sud, IN2P3/CNRS, F-91898 Orsay, France

[12],[*]University of Birmingham, Birmingham, B15 2TT, United Kingdom

[13],[*]Leibniz Universität Hannover, D-30167 Hannover, Germany

[14],[*]Albert-Einstein-Institut, Max-Planck-Institut für Gravitationsphysik, D-14476 Golm, Germany

[15],[*]Montana State University, Bozeman, MT 59717, USA

[16],[†]European Gravitational Observatory (EGO), I-56021 Cascina (Pi), Italy

[17],[*]LIGO - Hanford Observatory, Richland, WA 99352, USA

[18],[*]University of Glasgow, Glasgow, G12 8QQ, United Kingdom

[19],[*]University of Western Australia, Crawley, WA 6009, Australia

[20],[*]LIGO - Massachusetts Institute of Technology, Cambridge, MA 02139, USA

[21],[†]AstroParticule et Cosmologie (APC), CNRS: UMR7164-IN2P3-Observatoire de Paris-Université Denis Diderot-Paris VII - CEA : DSM/IRFU

[22],[*]Columbia University, New York, NY 10027, USA

[23],[†]National institute for subatomic physics, NL-1009 DB^a; Vrije Universiteit, NL-1081 HV ^{b}, Amsterdam, The Netherlands

[24],[*]The University of Texas at Brownsville and Texas Southmost College, Brownsville, TX 78520, USA

[25],[*]San Jose State University, San Jose, CA 95192, USA

[26],[*]Moscow State University, Moscow, 119992, Russia

[27],[†]ESPCI, CNRS, F-75005 Paris, France

[28],[*]LIGO - Livingston Observatory, Livingston, LA 70754, USA

[29],[*]Washington State University, Pullman, WA 99164, USA

[30],[†]INFN, Sezione di Perugia^a; Università di Perugia^b, I-6123 Perugia,Italy

[31],[*]University of Oregon, Eugene, OR 97403, USA

[32],[*]Cardiff University, Cardiff, CF24 3AA, United Kingdom

[33],[*]Syracuse University, Syracuse, NY 13244, USA

[34],[*]Rutherford Appleton Laboratory, HSIC, Chilton, Didcot, Oxon OX11 0QX United Kingdom

[35],[*]University of Maryland, College Park, MD 20742 USA

[36],[†]Laboratoire d'Annecy-le-Vieux de Physique des Particules (LAPP), IN2P3/CNRS, Université de Savoie, F-74941 Annecy-le-Vieux, France

[37],[*]University of Massachusetts - Amherst, Amherst, MA 01003, USA

[38],[†]INFN, Sezione di Firenze, I-50019 Sesto Fiorentino^a; Università degli Studi di Firenze, I-50121^b, Firenze; Università degli Studi di Urbino 'Carlo Bo', I-61029 Urbino^c, Italy

[39],[*]NASA/Goddard Space Flight Center, Greenbelt, MD 20771, USA

[40],[*]University of Michigan, Ann Arbor, MI 48109, USA

[41],[*]University of Sannio at Benevento, I-82100 Benevento, Italy

[42],[*]The University of Mississippi, University, MS 38677, USA

[43],[*]Charles Sturt University, Wagga Wagga, NSW 2678, Australia

[44],[*]Caltech-CaRT, Pasadena, CA 91125, USA

[45],[*]Carleton College, Northfield, MN 55057, USA

[46],[*]The University of Melbourne, Parkville VIC 3010, Australia

[47],[†]INFN, Sezione di Roma Tor Vergata[a]; Università di Roma Tor Vergata[b], Istituto di Fisica dello Spazio Interplanetario (IFSI) INAF[c], I-00133 Roma; Università dell'Aquila, I-67100 L'Aquila[d], Italy

[48],[*]Eötvös University, ELTE 1053 Budapest, Hungary

[49],[*]University of Salerno, 84084 Fisciano (Salerno), Italy

[50],[*]The University of Sheffield, Sheffield S10 2TN, United Kingdom

[51],[*]The Pennsylvania State University, University Park, PA 16802, USA

[52],[*]Inter-University Centre for Astronomy and Astrophysics, Pune - 411007, India

[53],[*]Southern University and A&M College, Baton Rouge, LA 70813, USA

[54],[*]California Institute of Technology, Pasadena, CA 91125, USA

[55],[†]Laboratoire des Matériaux Avancés (LMA), IN2P3/CNRS, F-69622 Villeurbanne, Lyon, France

[56],[*]University of Rochester, Rochester, NY 14627, USA

[57],[*]The University of Texas at Austin, Austin, TX 78712, USA

[58],[*]Australian National University, Canberra, 0200, Australia

[59],[*]Embry-Riddle Aeronautical University, Prescott, AZ 86301 USA

[60],[*]University of Minnesota, Minneapolis, MN 55455, USA

[61],[*]University of Adelaide, Adelaide, SA 5005, Australia

[62],[*]University of Southampton, Southampton, SO17 1BJ, United Kingdom

[63],[*]Universitat de les Illes Balears, E-07122 Palma de Mallorca, Spain

[64],[*]Northwestern University, Evanston, IL 60208, USA

[65],[*]National Astronomical Observatory of Japan, Tokyo 181-8588, Japan

[66],[*]Institute of Applied Physics, Nizhny Novgorod, 603950, Russia

[67],[*]University of Strathclyde, Glasgow, G1 1XQ, United Kingdom

[68],[*]Loyola University, New Orleans, LA 70118, USA

[69],[*]Hobart and William Smith Colleges, Geneva, NY 14456, USA

[70],[*]Louisiana Tech University, Ruston, LA 71272, USA

[71],[*]Andrews University, Berrien Springs, MI 49104 USA

[72],[*]Sonoma State University, Rohnert Park, CA 94928, USA

[73],[*]Trinity University, San Antonio, TX 78212, USA

[74],[*]Rochester Institute of Technology, Rochester, NY 14623, USA

[75],[*]Southeastern Louisiana University, Hammond, LA 70402, USA

[*]The LIGO Scientific Collaboration

[†]The Virgo Collaboration

Data Analysis Supplement

METHOD

Gravitational waves stretch and compress the spatial dimensions perpendicular to the direction of wave propagation. In a Michelson interferometer with suspended mirrors, the gravitational wave would cause stretching and shrinking of orthogonal arms, as shown in Figure 1, which would result in corresponding fluctuations in the laser intensity at the output of the interferometer. Hence, transient or periodic gravitational waves would cause transient or periodic fluctuations in the output laser power. A stochastic gravitational-wave background (SGWB) signal would cause random fluctuations in output laser power, which are indistinguishable from various instrumental noise sources. We hence search for a SGWB by cross-correlating strain data from pairs of interferometers, as described in [8]. In particular, we define the following cross-correlation estimator:

$$Y = \int_0^{+\infty} df\ Y(f) \tag{1}$$
$$= \int_{-\infty}^{+\infty} df \int_{-\infty}^{+\infty} df'\ \delta_T(f - f')\ \tilde{s}_1(f)^*\ \tilde{s}_2(f')\ \tilde{Q}(f'),$$

where δ_T is a finite-time approximation to the Dirac delta function, $\tilde{s}_1$ and $\tilde{s}_2$ are the Fourier transforms of the strain time-series of two interferometers, and $\tilde{Q}$ is a filter function. Assuming that the detector noise is Gaussian, stationary, uncorrelated between the two interferometers, and much larger than the GW signal, the variance of the estimator Y is given by:
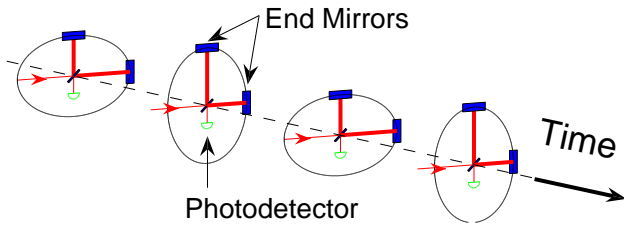
FIG. 1: **Effect of a gravitational wave on an interferometer.** A gravitational wave traveling perpendicular to the plane of the interferometer stretches and compresses interferometer arms in an alternating manner. The laser beam (entering from the left) is split equally between the arms, the two new beams travel to and reflect back from the end mirrors, and are superposed at the photo-detector (at the bottom). Changes in the arm lengths cause the two beams to acquire different phases while traveling in the arms, the differential component of which is observed as modulations in the laser light intensity at the photo-detector.

estimator Y is given by:

$$\sigma_Y^2 = \int_0^{+\infty} df\ \sigma_Y^2(f)$$
$$\approx \frac{T}{2} \int_0^{+\infty} df P_1(f) P_2(f)\ |\ \tilde{Q}(f)\ |^2, \tag{2}$$

where $P_i(f)$ are the one-sided strain power spectral densities (PSDs) of the two interferometers and T is the measurement time. Optimization of the signal-to-noise ratio leads to the following form of the optimal filter [8]:

$$\tilde{Q}(f) = \mathcal{N}\ \frac{\gamma(f)\Omega_{\mathrm{GW}}(f) H_0^2}{f^3 P_1(f) P_2(f)}, \tag{3}$$

where H_0 is the present value of the Hubble parameter, assumed below to take the value $H_0 = 72$ km/s/Mpc [19], and $\gamma(f)$ is the overlap reduction function [8], arising from the overlap of antenna patterns of interferometers at different locations and with different orientations. For the Hanford-Livingston pairs the sensitivity above 50 Hz is attenuated due to the overlap reduction, while the identical antenna patterns of the colocated Hanford interferometers imply $\gamma(f) = 1$. Hence, the colocated Hanford interferometer pair is more sensitive to the isotropic SGWB than the Hanford-Livingston pairs, but it is also more susceptible to environmental and instrumental correlations. For this reason, this pair is not included in the analysis presented here. Since most theoretical models in the LIGO frequency band are characterized by a power law spectrum, we assume a power law template GW spectrum with index α,

$$\Omega_{\mathrm{GW}}(f) = \Omega_\alpha \left(\frac{f}{100\ \mathrm{Hz}}\right)^\alpha. \tag{4}$$

The normalization constant $\mathcal{N}$ in Equation 3 is chosen such that $< Y >= \Omega_\alpha$.

RESULTS

Our results are based on the LIGO data acquired during the science run S5, which took place between November 5, 2005 and September 30, 2007. Virgo [19] and GEO [20] detectors were also operating during some parts of this science run. However, due to their lower strain sensitivities around 100 Hz, these interferometers were not included in the search presented here. We analyzed the H1-L1 and H2-L1 interferometer pairs. The data for each interferometer pair was divided into 60 sec segments, downsampled to 1024 Hz, and high-pass filtered with a 6th order Butterworth filter with 32 Hz knee frequency. Each
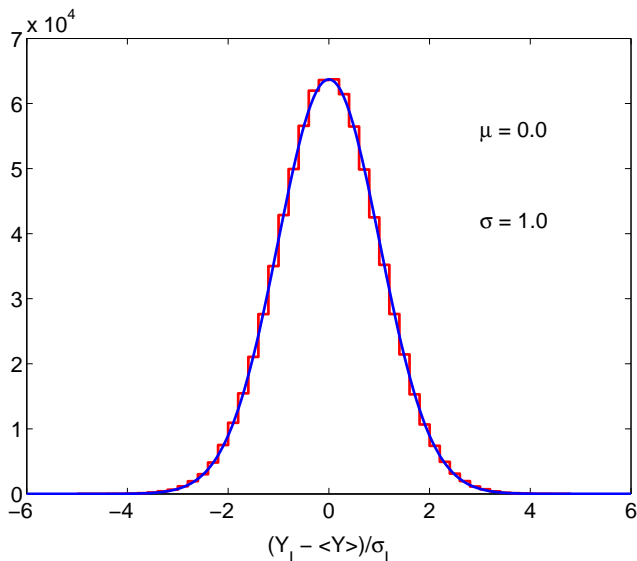
FIG. 2: Histogram of the fluctuations of the estimator Y_I over segments I around the mean, normalized by the standard deviation σ_I is shown in red (for the H1-L1 pair). The blue curve shows the Gaussian fit to the histogram, which has zero mean and unit variance. The Kolmogorov-Smirnov test statistic (comparing the histogram and the fit) is 0.2 for H1-L1 (0.4 for H2-L1), indicating that the data is indeed Gaussian-distributed, and that the estimate of the theoretical variance σ_I^2 is reliable.

segment I was Hann-windowed and estimators $Y_I(f)$ and $\sigma_I(f)$ were evaluated with 0.25 Hz resolution. To recover the loss of signal-to-noise due to Hann-windowing, segments were 50% overlapped. A weighed average was performed over all segments from both interferometer pairs, with inverse variances as weights.

The data were preselected to avoid digitizer saturation effects, periods with unreliable calibration, and periods suffering from known instrumental transient disturbances. In addition, about 3% of the segments were found to deviate from the assumption of stationary noise: the difference between σ_I and σ calculated using the neighboring segments exceeded 20% for these segments, and they were not included in the analysis. The 20% threshold is optimal as it yields gaussian distribution of the data (c.f. Figure 2), while minimizing the amount of eliminated data. The data quality selection was performed blindly, using an un-physical 0.5-sec time-shift between the two interferometers (a broadband SGWB covering the range of ~ 100 Hz is expected to have coherence time ~ 10 ms, as also depicted in Figure 5). Once the data selection was completed, the final zero-lag analysis was performed. The selected segments amount to 292 days of exposure time for H1-L1 (294 days for H2-L1).

To identify potentially contaminated frequency bins, we calculated the coherence between H1 and L1 (and H2 and L1) over the entire S5 run. The coherence is defined
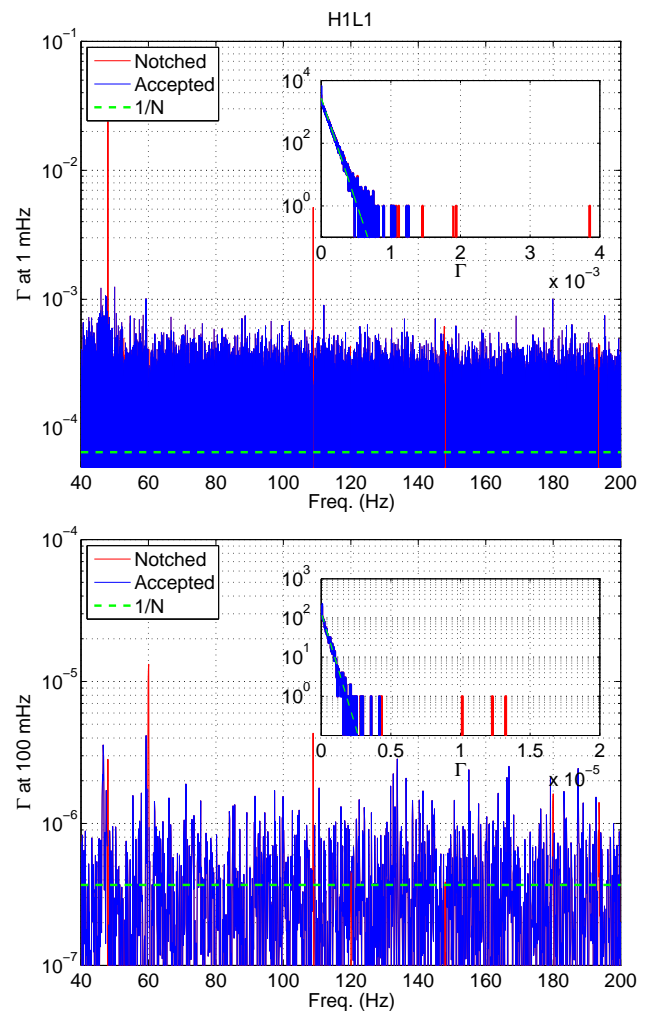

FIG. 3: Coherence between H1 and L1 strain data is shown at 1 mHz resolution (top) and 100 mHz resolution (bottom). The insets show the histograms of the coherence along with the expected exponential distribution. Note that after notching the contaminated bins (red), the remaining frequencies follow the expected exponential distribution. Note: N denotes the number of averages used in the calculation.

as

$$\Gamma(f) = \frac{|\langle P_{12}(f)\rangle|^2}{\langle P_1(f)\rangle \langle P_2(f)\rangle}, \tag{5}$$

where $\langle P_{12}(f)\rangle$ is the average strain cross-spectral density between two interferometers and $\langle P_i(f)\rangle$ is the average strain power-spectral density for the interferometer i. These calculations have revealed several instrumentally correlated lines between each pair of interferometers: 16 Hz harmonics (associated with the data acquisition clock), 60 Hz harmonics (AC power line), and injected simulated pulsar signals (52.75 Hz, 108.75 Hz, 148 Hz, 193.5 Hz, and 265.5 Hz). These lines were found to be correlated between instruments in the blind analysis, and were excluded from the final zero-lag analysis.
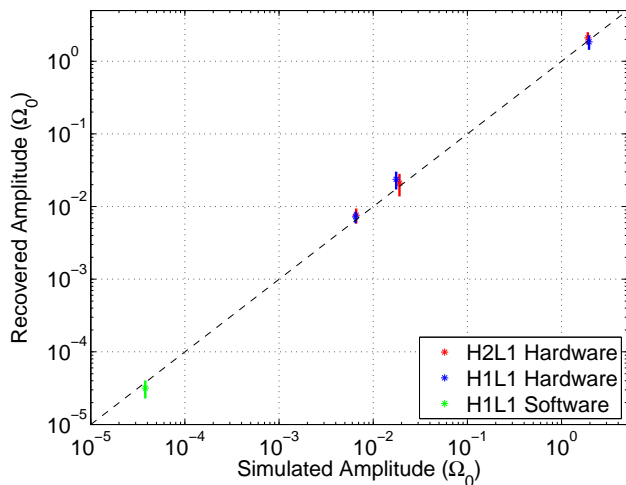
FIG. 4: Stochastic signal simulations in hardware for H1-L1 (blue) and H2-L1 (red), and in software (H1-L1, green) are shown. The error bars denote 2σ ranges.
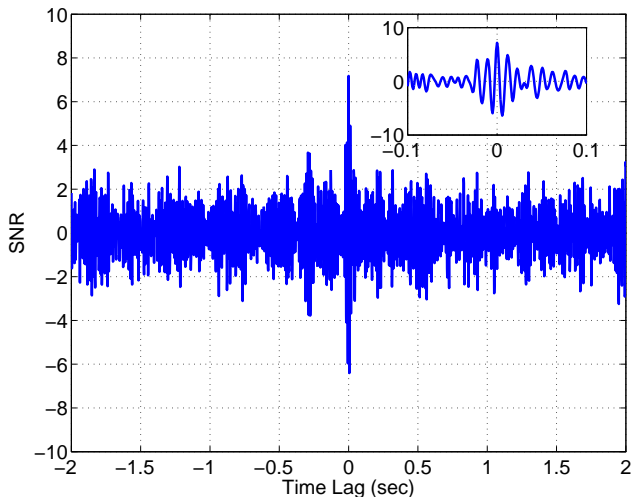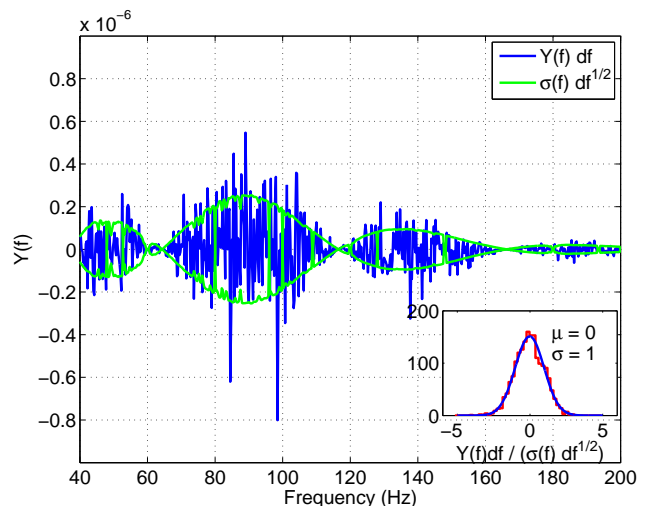

FIG. 6: $Y(f)$ and $\sigma(f)$ obtained by combining the H1-L1 and H2-L1 data from the S5 run. The inset shows that the ratio of the two spectra is consistent with a Gaussian of zero mean and unit variance.

FIG. 5: Signal-to-noise ratio for the recovery of a software simulation with H1-L1 data with $\Omega_0^{simulated} = 3.8 \times 10^{-5}$ is shown as a function of the time-lag between the two interferometers. The inset shows the zoom-in around zero-lag: the signal is recovered well for zero-lag (SNR ≈ 7.2), but it disappears quickly with time-lag of ± 30 ms.
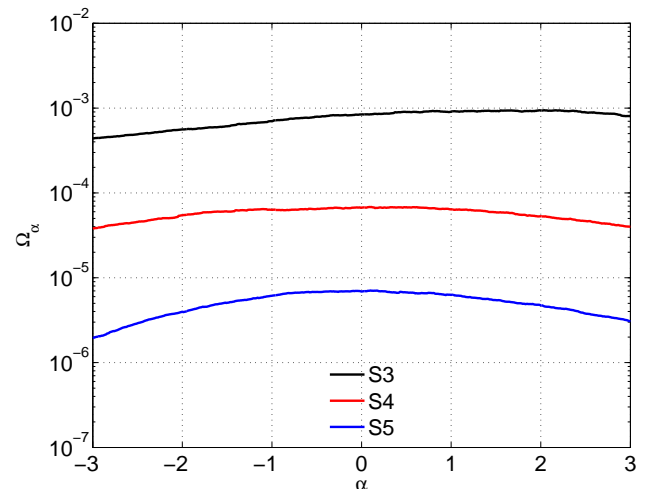

FIG. 7: Upper limit is shown as a function of the power index α for several LIGO results: based on the previous runs S3 and S4 and the S5 result presented here.

Figure 3 shows the coherence between H1 and L1 strain data at 1 mHz and 100 mHz resolutions.

The search algorithm described here is verified using signal simulations. The simulations are performed in hardware (by physically moving the interferometer mirrors coherently between interferometers), in which case they are short in duration and strong in amplitude. They are also performed in software, by adding the stochastic signal to the interferometer data, in which case they can be long in duration and relatively weak in amplitude. Three hardware simulations were performed, with amplitudes of $\Omega_0 \approx 2$ (20 min long), 2×10^{-2} (20 min long), and

6.5×10^{-3} (~ 3.8 hours long) and they were successfully recovered (within experimental uncertainties) for both H1-L1 and H2-L1 pairs. A software simulation was performed and successfully recovered using about $1/2$ of the H1-L1 data, with the amplitude of $\Omega_0 = 3.8 \times 10^{-5}$. Figures 4 and 5 demonstrate the recovery of both hardware and software simulations.

We apply the above search technique to the data acquired by LIGO during the science run S5, repeating it for the interferometer pairs H1-L1 and H2-L1. We treat the data from the two pairs as uncorrelated, although H1 and H2 are known to suffer from instrumental and environmental correlations. We have verified

that the level of the H1-H2 correlations is sufficiently small that it could affect the result presented here by less than 1%. The resulting composite spectrum for the frequency independent template ($\alpha = 0$) is shown in Figure 6. Integrated over the frequency band 41.5-169.25 Hz, which contains 99% of the sensitivity as determined by the variance integrand, this leads to the final point estimate for the frequency independent GW spectrum: $\Omega_0 = (2.1 \pm 2.7) \times 10^{-6}$, where the quoted error is statistical. We calculate the Bayesian posterior distribution for Ω_0 using this result. For the prior distribution of Ω_0 we use our previously published posterior distribution from the earlier S4 run [22]. We also marginalize over the calibration uncertainty, which is the dominant systematic error in this analysis and was estimated to be 13.4% for L1 and 10.3% for H1 and H2. With these assumptions, the final 95% confidence upper limit is $\Omega_0 < 6.9 \times 10^{-6}$. Figure 7 shows the 95% confidence upper limit as a function of the power index α of the template spectrum. This result is more than an order of magnitude improvement over the latest LIGO result in this frequency region [22].

OUTLOOK

LIGO and Virgo are planning significant upgrades to their interferometers, known as Advanced LIGO and Advanced Virgo. These upgrades will improve the interferometers' strain sensitivities by 10 times across the entire frequency band, and they will extend the sensitive frequency band down to ~ 10 Hz. Consequently, the network of advanced detectors will be able to probe the isotropic SGWB at the level of $\Omega_{GW} \sim 10^{-9}$ or better. Moreover, while searches for isotropic SGWB tend to be dominated by pairs of nearby or co-located detectors, the presence of the third location in the network is crucial for searches for non-isotropic SGWB. Hence, the network of advanced detectors is expected to produce detailed maps of the gravitational-wave sky, potentially revealing non-isotropic sources of SGWB, such as point sources or sources distributed in the galactic plane. Techniques for performing the searches for non-isotropic SGWB are currently under development.

Author Contributions: The LIGO Scientific Collaboration (LSC) and the Virgo Collaboration are organized into several working groups, each focusing on a different aspect of the experiment. Each author is associated with one or more of these groups. Moreover, all of the authors participated in the acquisition of the data that led to this letter. As described in the MoU between the LSC and Virgo, there are joint data analysis groups: the Burst Search Group (chairs E. Katsavounidis, P. Shawhan and P.Hello) performs searches for transient signals; the Compact Binary Coalescences Search Group (chairs S. Fairhurst, A. Weinstein and F. Marion) performs searches for compact binary coalescence signals; the Continuous-Waves Search Group (chairs K. Riles, G. Woan and C. Palomba) performs searches for continuous periodic signals; the Stochastic Search Group (chairs S. Ballmer, V. Mandic and G. Cella) performs searches for stochastic signals and is responsible for the analysis that led to the result presented here and for writing of this letter. The Stochastic Review Committee (chairs W. Anderson and F. Ricci) has conducted an extensive internal review of the method and the results presented in this letter. Similar review committees exist for the Burst, Compact Binary Coalescences, and Continuous-Waves groups. The Data Analysis Council (chairs M.A. Papa and G. Guidi) coordinates different analysis efforts. On the LIGO side the Detector Characterization Group (chair G. Gonzalez) performs studies of LIGO detector performance; Calibration Group (chairs K. Kawabe and X. Siemens) establishes the calibration of LIGO detectors. On the Virgo side the Reconstruction group (coordinator L. Rolland) provides a reconstructed and calibrated strain measurement while the Noise Study group (coord. E. Cuoco) studies the noise present in the detector. The Commissioning group (coord. E. Calloni) establishes proper detector tuning. The Detector Group (coord. P. Rapagnani) organizes detector operations and upgrades. The Director of the LIGO Laboratory is J. Marx, the Deputy Director is A. Lazzarini, and the LSC spokesperson is D. Reitze. The Virgo Spokesperson is F. Fidecaro.